minerals

MDPI

Article

Evolution from Carbonate Platform to Pelagic Environments in the South Iberian Paleomargin (Pliensbachian–Early Toarcian, Early Jurassic): Carbonate Features and Isotope Geochemistry

Luis M. Nieto [1,*], José M. Molina [1], Pedro A. Ruiz-Ortiz [1], Ángela Fraguas [2] and Matías Reolid [1]

[1] Department of Geology and Center of Advanced Studies in Earth Sciences, Energy and Environment (CEACTEMA), University of Jaén, Campus Universitario Las Lagunillas, 23071 Jaén, Spain; jmmolina@ujaen.es (J.M.M.); paruiz@ujaen.es (P.A.R.-O.); mreolid@ujaen.es (M.R.)

[2] Department of Biology, Geology, Physics and Inorganic Chemistry and Research Group in Earth Dynamics and Landscape Evolution (DYNAMICAL), University King Juan Carlos, 28933 Móstoles, Spain; angela.fraguas@urjc.es

* Correspondence: lmnieto@ujaen.es

Abstract: This paper studies ten Subbetic (Betic External Zones) stratigraphic sections spanning the Pliensbachian–early Toarcian time interval. Eight lithofacies were distinguished: crinoidal limestones, peloidal limestones, breccias, cherty limestones, nodular limestones, hardground surfaces and condensed levels, marls and marly limestone alternance, and dark marls. The biostratigraphy matches data from ammonite and calcareous nannofossil zonations. In addition, we analyzed C and O isotopes from bulk samples from three of the studied sections in which the lower Toarcian sedimentation crops out. The demise of the Lower Jurassic shallow platform developed in the South Iberian Paleomargin was a complex process driven by rifting, which led to tilted blocks giving way to different sedimentary environments. The tectonic stages occurred in the Sinemurian–Pliensbachian transition (R1), toward the lower part of the Ibex Zone (FO of the *Biscutum grande*, R2), in the Ibex–Davoei zones boundary (FO of *Lotharingius barozii*, R3), in the lower–upper Pliensbachian (R4), and in the lower boundary of the NJT4d nannofossil Subzone (R5) (Lavinianum Zone, upper Pliensbachian). After this last phase, sedimentation became pelagic in origin throughout the basin, represented by the sections studied. However, the isotope data show no clear record of the different C-isotopic events, though the Davoei–Margaritatus Event, the late Pliensbachian Event, and the Pliensbachian–Toarcian Boundary Event (PTBE) could be cautiously identified. These geochemical features are explained by the convergence of marine currents from Panthalassa (through the Hispanic Corridor) and Tethys.

Keywords: Early Jurassic; South Iberian Paleomargin; Subbetic; facies analysis; carbonate isotope geochemistry; synsedimentary tectonics; demise of the platform

Citation: Nieto, L.M.; Molina, J.M.; Ruiz-Ortiz, P.A.; Fraguas, Á.; Reolid, M. Evolution from Carbonate Platform to Pelagic Environments in the South Iberian Paleomargin (Pliensbachian–Early Toarcian, Early Jurassic): Carbonate Features and Isotope Geochemistry. *Minerals* **2023**, *13*, 1386. https://doi.org/10.3390/min13111386

Academic Editor: Marco Taviani

Received: 4 October 2023
Revised: 22 October 2023
Accepted: 25 October 2023
Published: 29 October 2023

1. Introduction

In the Pliensbachian stratigraphic record of the southern and northern paleomargins of the Tethys, several perturbations in the C cycle have been detected, interpreted as major paleoenvironmental changes [1,2] from the analysis of sedimentological, mineralogical, or geochemical proxies [3–9]. In this sense, five isotopic events have been distinguished along the Pliensbachian [10]: (1) the Sinemurian–Pliensbachian Boundary Event (SPBE), (2) the Ibex Zone Event, (3) the Davoei–lower part of the Margaritatus zones Event, (4) the Margaritatus Zone Event, and (5) the end of the Margaritatus–Spinatum Event. In addition, the Pliensbachian–Toarcian Event (Pl-To), preceding the Toarcian Oceanic Anoxic Event (T-OAE), has also been recognized [2,11–14].

The SPBE has been interpreted as a change in the C isotopic composition of the ocean–atmosphere system coinciding with changes in the shallow-water carbonate pattern [1,15,16]. The factors that induced this isotopic change are unclear, but they have been associated

with hydrothermal activity during the early stages of the break-up of Pangea and the opening of the Hispanic Corridor. These volcanic processes have been associated with the activity of the Central Atlantic Magmatic Province [6].

From the study of clay mineralogy and isotopic content, it has been established that significant temperature and moisture variations occurred along the Pliensbachian [8,9,17–20], reflecting successive warm/wet and cold/dry episodes that could reflect different stages in the development of ice caps.

The Pl-To Event has been characterized by a reduction in carbonate platform production linked to a crisis in calcareous nannoplankton [21–26], which resulted in the sedimentation of mostly marls. This event has been associated with the onset of the Karoo–Ferrar Large Igneous Province [27–29].

In the South Iberian Paleomargin (SIP), the SPBE took place during a broad transgression that affected the western margins of the Tethys. This transgression could be associated with the initial break-up of the carbonate platform developed between the Hettangian and the Pliensbachian, represented by the Gavilán Formation (Fm) [30,31]. As a consequence of this tectonic stage, the platform was configured with an irregular topography, showing differential subsidence between adjacent blocks. The accumulation of pelagic and hemipelagic sediments, which characterize the Zegrí Fm, was favored in the more subsiding areas of the grabens [32]. According to the previous authors, the break-up process started in the early Pliensbachian, while the drowning of the platform was dated to the late early Pliensbachian. More recently, a composite model has been proposed to explain the demise of the Lower Jurassic peritethys platforms [33]. This model assumes that the disappearance of the shelves was the result of (1) extensional tectonic processes and a eustatic sea level fall that occurred in the latest Sinemurian, and (2) successive phases of flooding in which ocean acidification and a drop in carbonate saturation of the shallow platforms resulted in the development of unfavorable conditions for carbonate factory (calcite and aragonite).

The main goal of the present paper is to establish, with the highest precision, the factors that triggered the demise of the carbonate platform in the SIP during the Pliensbachian and to analyze the C and O isotopic record in the sediments developed after its disappearance in order to determine the paleoenvironmental conditions that settled in the paleomargin after this demise.

2. Geological Setting

The Betic External Zones (BEZ; Figure 1) comprises sedimentary rocks deposited in the SIP during the Alpine tectonic cycle (Mesozoic–Early Miocene). The SIP had a WSW-ENE trend (Figure 1A,B). The N-NE part of the BEZ is constituted by the Prebetic, made up of para-autochthonous units and overlain by the allochthonous units of southern provenance that form the Subbetic. The latter domain consists of predominantly pelagic/hemipelagic sediments deposited after the break-up of the carbonate platform developed during the earliest Jurassic (Hettangian–Pliensbachian) at the Northern margin of the Western Tethys [31,34–38]. The rocks representing this carbonate platform make up the Gavilán Fm, while the overlying pelagic/hemipelagic rocks constitute the Zegrí Fm [36,38–41]. The Gavilán Fm overlies the Upper Triassic materials of Keuper facies with a contact generally affected by alpine tectonics. Three members have been differentiated within the Gavilán Fm [31]: the lower one consists of algal laminite facies, the middle one is composed of oolitic limestones, and the upper one is where crinoid and cherty limestones predominate. Between the lower and middle members, a stratigraphic discontinuity (R1) with an associated hiatus of variable duration has been recognized [31]. Moreover, these authors identified another discontinuity, with an associated hiatus covering part of the Ibex Zone between the middle and upper members of Gavilán Fm (R2). Finally, at the top of the third member, which coincides with the top of this lithostratigraphic unit, another stratigraphic unconformity has been identified by the same authors (R3), with an associated hiatus of uncertain duration, including at least the Davoei Zone [31]. In this paper, two

additional unconformities are proposed between the top of the Gavilán Fm and the base of the Zegrí Fm, named R4 and R5, which will be analyzed in detail in the 4.3 Section.

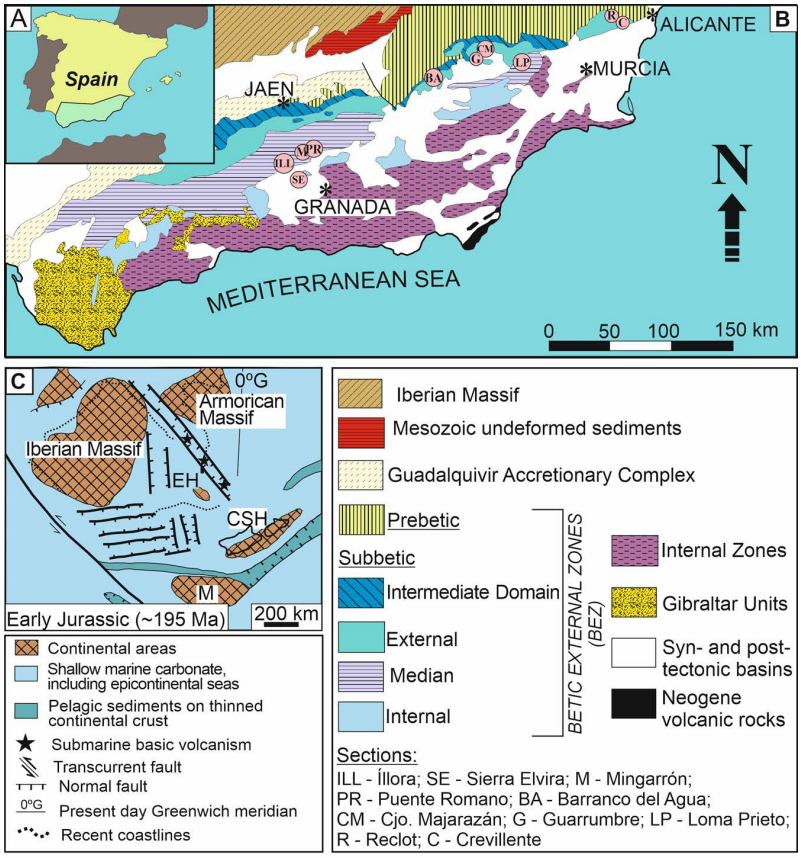

Figure 1. Geographical and geological location of the studied sections. (**A**) Location of the Betic Cordillera in the South of Spain. (**B**) Geological scheme of the Betic Cordillera highlighting the Betic External Zones, especially the Subbetic. (**C**) Paleogeographic reconstruction of the Iberian Microplate in the Early Jurassic [35,36]. M: Mesomediterranean Microplate; CSH: Corsica–Sardinia High; EH: Ebro High; ILL: Íllora section; SE: Sierra Elvira section; M: Mingarrón section; PR: Puente Romano section; BA: Barranco del Agua section; CM: Cortijo (Cjo.) Majarazán section; G: Guarrumbre section; LP: Loma Prieto section; R: Reclot section; and C: Crevillente section.

The Zegrí Fm, made up of hemipelagic/pelagic materials, lies on top of the Gavilán Fm. Five types of lithofacies are differentiated within the Zegrí Fm [42]: (1) grey-yellow marl–marly limestone rhythmite and limestones in the uppermost Pliensbachian to lowermost Toarcian (lower part of the Polymorphum Zone); (2) dark marls (upper part of the Polymorphum Zone and lower part of the Serpentinum Zone); (3) thin-bedded grey-yellow limestones, locally with chert and abundant slumps (upper part of the Serpentinum Zone); (4) grey marls with some marly limestones of the middle Toarcian (Bifrons and Gradata zones); and (5) yellow or brown laminated calcisiltites and fine calcarenites that occur intercalated in lithofacies 3 and 4.

3. Materials and Methods

3.1. Fieldwork and Facies Analysis

Ten stratigraphic sections were selected from the Subbetic (Figures 1 and 2) in which the contact between the Gavilán and Zegrí Fms (generally intra-Pliensbachian) is well exposed. In addition, in three of them, the contact between Pliensbachian and lower Toarcian rocks has been detected. Samples were collected for facies and microfacies analysis. A Leica M205C binocular microscope was used to study the microfacies from 250 thin sections. Ammonites were collected for dating rocks. The biozonation proposed by Hesselbo et al. [43]

for the Tethyan Domain has been considered for ammonite biostratigraphy. In addition, samples of the Guarrumbre (G) section were taken for dating with calcareous nannofossils, considering the biostratigraphic scale proposed by Ferreira et al. [44] for the Tethyan Domain. On the other hand, the Illora (ILL), Sierra Elvira (SE), Mingarrón (M), Bco. del Agua (BA), Cortijo Majarazán (CM), Loma Prieto (LP), Reclot (R), and Crevillente (C) sections were studied by Nieto et al. [37] in order to compare the ammonite biostratigraphy to the results obtained from Sr-Isotope Stratigraphy (SIS) based on the methodology proposed by McArthur et al. [45]. Therefore, the chronostratigraphy used in these sections is based on the results obtained by Nieto et al. [37].

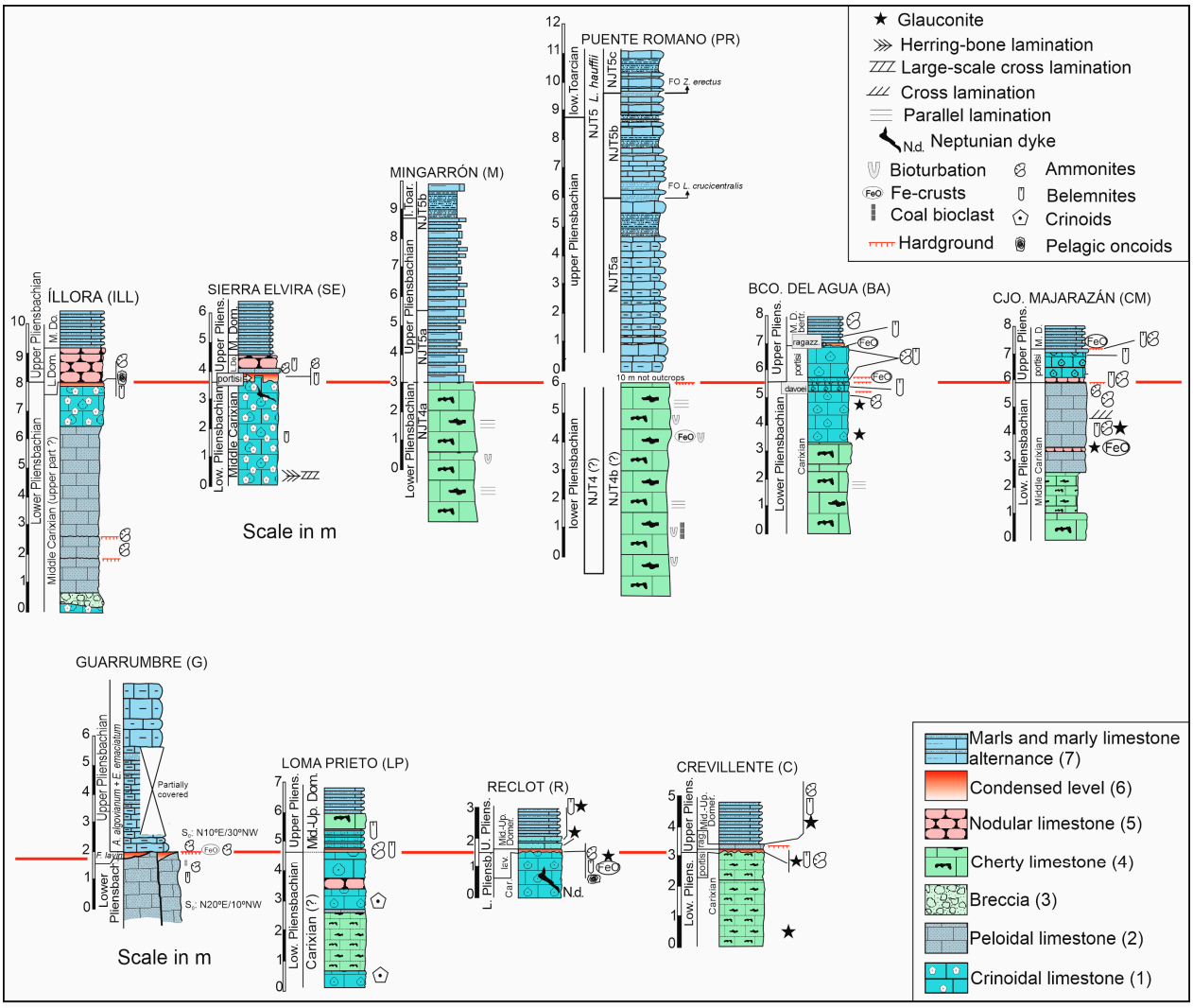

Figure 2. Correlation of the stratigraphic sections considered in this paper. The red line marks the boundary between the lower and upper Pliensbachian.

The orientation of the belemnites observed on the omission surfaces and hardgrounds of the Guarrumbre (G) and Reclot (R) sections was measured in outcrop with a Wilkie compass. The strike of the major axis of these fossils, measured clockwise, has been considered to follow the orientation of the apex of the rostrum [46]. These data were plotted in a rose diagram, using the Stereonet software.

3.2. C and O Isotope Geochemistry

The C and O isotopes were systematically analyzed from bulk samples from the Mingarrón (M), Puente Romano (PR), and Guarrumbre (G) sections (Table S1). The milled

samples were analyzed at the Laboratory of the Scientific and Technological centre (CCiT) of the University of Barcelona with a Finningan MAT 253 isotope ratio mass spectrometer with a Kiel IV carbonate analysis device (ThermoFisher Scientific, Waltham, MA, USA). The isotope ratios obtained refer to the VPDB standard notation in ‰. Analytical precision was kept between 0.01 and 0.05 for $\delta^{13}C$ and $\delta^{18}O$, respectively.

3.3. Calcareous Nannofossils

In terms of calcareous nannofossils, 38 smear slides from the Guarrumbre (G) section were prepared following the standard technique of Bown and Young [47] and the corresponding semi-quantitative analyses were performed with a Leica DMLP light microscope equipped with a Leica DFC 420 digital camera at 1250× magnification. Four transverses were analyzed in each slide, resulting in more than 500 fields of view, in order to identify those species that are rare or very rare. Total abundance and degree of preservation of calcareous nannofossil assemblages, as well as the relative abundances of each species identified, were determined following the criteria of Perilli et al. [48] (Table S2 shows the distribution chart). An alphabetical listing is shown in Appendix A that includes all the calcareous nannofossil species cited in the text with full author citations.

4. Results

4.1. Biostratigraphy and Chronostratigraphy

The ammonite biozonation proposed by Hesselbo et al. [43] coincides with that previously proposed by Braga [49] for the upper Pliensbachian (Domerian) of the Subbetic, which was also reported in Nieto et al. [37]. Regarding the ammonite biozonation from the lower Toarcian, herein those biostratigraphic schemes of Jiménez [50], Sandoval et al. [51], and Reolid et al. [52] are considered for the Subbetic, which slightly differ from that proposed by Hesselbo et al. [43] for the Tethyan Domain. They considered that the first biozone is *Dactylioceras tenuicostatum*, whilst in the Subbetic, the first biozone recorded in the lower Toarcian is *Dactylioceras* (*E.*) *polymorphum*. It is noteworthy that the Polymorphum Zone corresponds to the Mediterranean biozonation proposed by Elmi et al. [53] and Page [54].

In the Subbetic, the lower Pliensbachian is poorly identified due to the scarcity of ammonites. In the ILL section, the presence of *Tropidoceras mediterraneum* has been recorded, with specimens identified as belonging to the Ibex Zone [37]. Several authors (see [37] for more details) show that the different regional studies carried out in this geological domain reveal the general absence of ammonites attributable to the Davoei Zone (Figure 3). For the upper Pliensbachian, the presence of *Fieldingiceras fieldingii*, *Fuciniceras isseli*, *Fuciniceras fucini*, and *Protogrammoceras celebratum* in SE, M, BA, CM, and C sections has been recorded, which characterize the Portisi Subzone (lowermost part of the Lavinianum Zone) [37]. The Algovianum and Emaciatum zones have been recognized in regional studies [37,38].

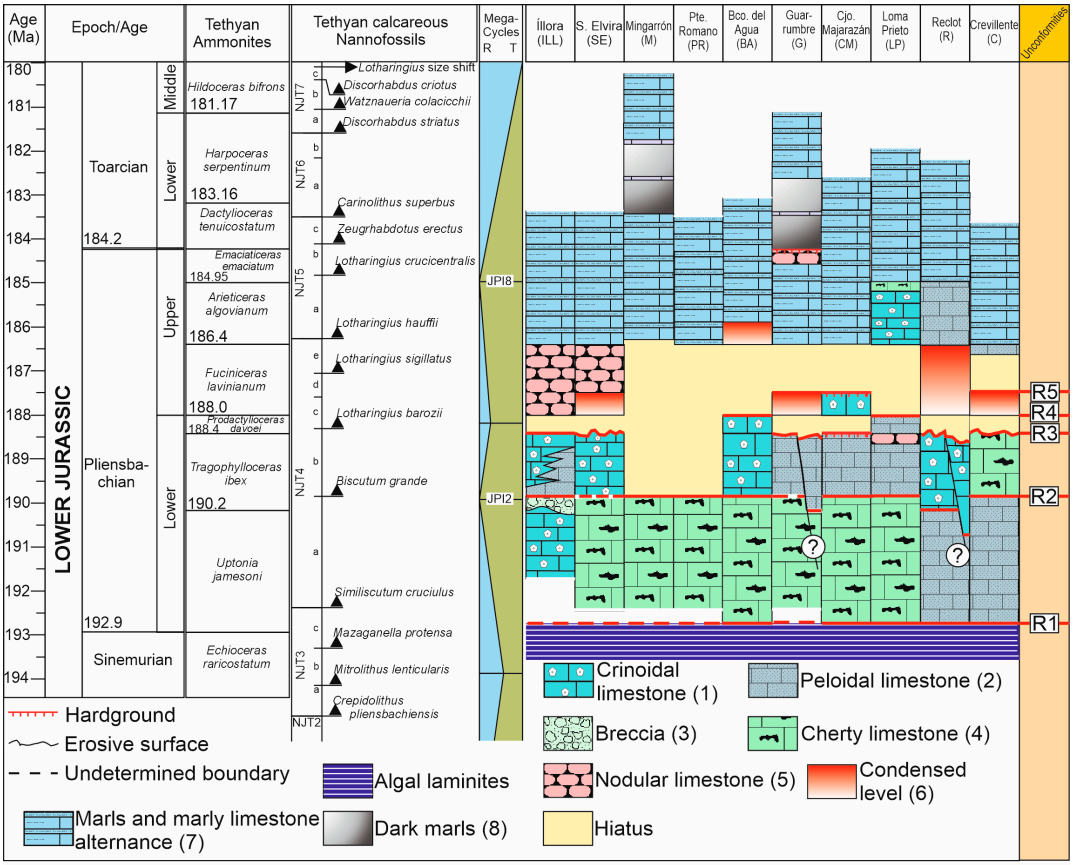

Figure 3. Chronostratigraphic scheme for the Lower Jurassic (Pliensbachian–lower Toarcian) from the data obtained in the stratigraphic sections of the Subbetic considered in this paper. The numerical ages and the Tethyan Ammonites zones are from Hesselbo et al. [43]. The Tethyan calcareous nannofossils are from Hesselbo et al. [43] and Ferreira et al. [44].

With respect to the upper Pliensbachian–lower Toarcian calcareous nannoplankton, in the M, PR, and G sections, the NJT5a (upper Pliensbachian) and NJT5b (comprising the uppermost part of the Pliensbachian and the lowermost Toarcian, Tenuicostatum Zone) subzones have been identified based upon the first occurrences (FO) of *Lotharingius hauffii* and *Lotharingius crucicentralis*, respectively. In the M section, the NJT6 Zone has been directly identified over the NJT5b Subzone [55], considering the FO of *Carinolithus superbus*, spanning almost the entire lower Toarcian, which can be correlated with the upper part of the Tenuicostatum Zone and most of the Serpentinum Zone (Figure 3). On the other hand, in the PR section, above the NJT5b Subzone, the NJT5c Subzone has been identified based upon the FO of *Zeugrhabdothus erectus*, which enabled the approximation of the upper Pliensbachian/lower Toarcian boundary [56].

The relatively abundant and moderately preserved calcareous nannofossil assemblages from the G section analyzed for this paper are constituted by a total of 30 species belonging to 15 genera (check the distribution chart, Supplementary Materials, Table S2, for further details and Appendix A). Nannofossil assemblages are mainly dominated by *Schizosphaerella punctulata*, *Calcivascularis jansae*, and *Lotharingius hauffii*. Four calcareous nannofossil subzones have been identified considering the biostratigraphic scheme of Ferreira et al. [44]: NJT5a, NJT5b, NJT5c, and NJT6a, and, consequently, three primary or zonal events have been recognized: the FO of *Lotharingius crucicentralis* (Emaciatum Zone, upper Pliensbachian), the FO of *Zeugrhabdotus erectus* (Emaciatum/Polymorphum zonal boundary, uppermost Pliensbachian), and the FO of *Carinolithus superbus* (Polymorphum Zone, lower Toarcian).

Considering the ammonites collected and the results obtained from the SIS, the dating of the CM section was refined [37] so that the peloidal limestones should belong to the Luridum Subzone (the latest part of the Ibex Zone) and the overlying crinoidal limestones should belong to the upper part of the Portisi Subzone and the lower part of the Cornacaldense Subzone (upper part of the Lavinianum Zone).

In the same way, the crinoidal limestones from the BA section should belong to the upper part of the Figulinum Subzone and the terminal part of the Portisi Subzone, that is, the final part of the Davoei Zone and the lower part of the Lavinianum Zone [37].

From the above data, it can be generalized that in the lower–upper Pliensbachian transition in the Subbetic, a hiatus with a variable extension can be detected and correlated between the different stratigraphic sections considered in this paper. The greatest extent of the hiatus is detected in the M and PR sections, where the interval between the Ibex and Laviniaum zones, both included, is not represented (Figure 3). The smallest extent of the hiatus is recorded in the ILL, SE, G, CM, and R sections, where there is no representation of the Davoei Zone (Figure 3). Finally, at the BA, G, CM, LP, and C sections, the hiatus also encompasses the Davoei and Lavinianum zones (BA and LP sections), the middle and upper part of the Lavinianum Zone (G, CM, and C sections), and the Lavinianum Zone (G, CM, and C sections).

4.2. Facies Analysis

In the studied sections (Figure 2), eight lithofacies could be distinguished in the Pliensbachian and lower Toarcian materials (see description of the facies in Table 1 and microfacies in Figure 4). In the lower Pliensbachian (Jamesoni Zone), a lithofacies of cherty limestones (lithofacies 4 in Table 1; Figure 4A) is the most abundant and was recorded at the M, PR, BA, CM, and LP sections (Figures 2 and 3). However, in the C section, this lithofacies seems to belong to the Ibex Zone (lower Pliensbachian; Figure 3); in this section, the top of this lithofacies clearly shows an erosive irregular geometry.

Table 1. Lithofacies types recorded in the stratigraphic sections studied.

No.	Lithofacies	Textural Grains and Biota	Environment
1	Crinoidal limestone (grainstone)	Crinoids, peloids, ooids, and bioclasts. Cross-lamination (megaripples and herringbone lamination in Sierra Elvira section). Benthonic foraminifera.	High-energy open platform
2	Peloidal limestone (packstone/grainstone)	Peloids, crinoids, ooids, bioclasts, sponge spicules. Bivalves.	Low-energy platform
3	Breccias	The texture of the clasts is wackestone/packstone of peloids, crinoids, or bioclasts. They are enclosed in a mudstone/wackestone matrix with some crinoidal bioclasts, radiolaria, and sponge spicules.	High-energy platform. Reworking of the previous lithofacies
4	Cherty limestones (mudstone/wackestone)	Sponge spicules, radiolaria, peloids, and undetermined bioclasts.	Open platform or hemipelagic
5	Nodular limestones (wackestone/packstone)	Truncate ammonites, belemnites, bivalve bioclasts, crinoids, and benthonic foraminifera (Involutina liassica, Vidalina martana). Irregular surfaces. Thin Fe-crusts.	Hemipelagic
6	Hardground and condensed levels	Irregular surfaces stained by Fe-crusts (mm to cm thickness). Ammonites and belemnites.	Hemipelagic
7	Marls and marly limestone (mudstone) alternance	Sponge spicules and some bioclasts. Local belemnites and ammonites.	Hemipelagic/pelagic
8	Dark marls	Faint parallel lamination.	Hemipelagic/pelagic

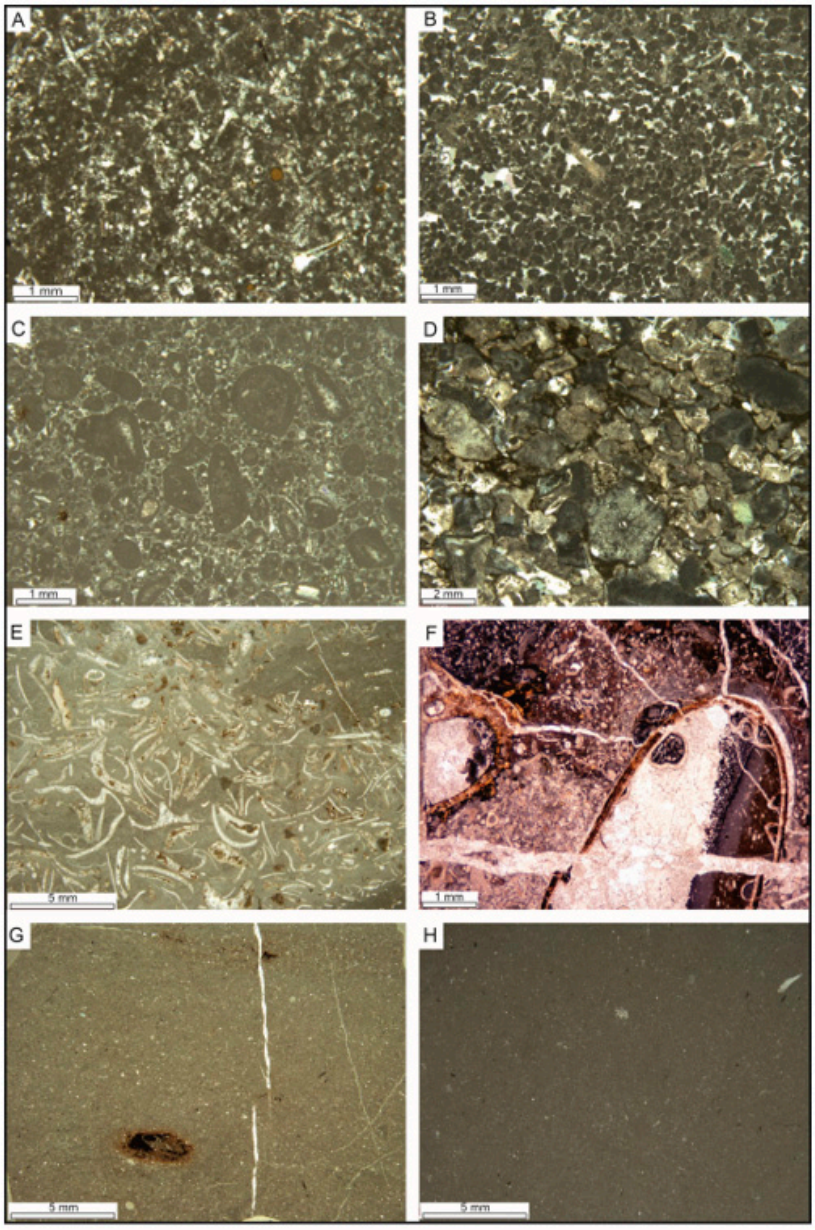

Figure 4. Microfacies. (**A**) Sponge spicules wackestone (cherty limestones). (**B**) Peloidal packstone (peloidal limestones). (**C**) Peloidal packstone with ooids (peloidal limestones). (**D**) Crinoidal grainstone (crinoidal limestones). (**E**) Bivalve packstone (nodular limestones). (**F**) Condensed level with ammonite sections and thin Fe-crusts coating the ammonites. (**G**) Mudstone with Fe-nodule. (**H**) Mudstone with some unclassified bioclasts.

In the ILL, SE, BA, and R sections (Figures 2 and 3), the dominant lithofacies is crinoidal limestones (lithofacies 1 in Table 1; Figure 4D). In the ILL section, this lithofacies has been recorded both in the Jamesoni Zone and in the upper part of the Ibex and Davoei zones. However, at the ILL section in the Jamesoni Zone, a level with an erosional bottom made up of breccias mainly of peloidal–oolitic limestone clasts (lithofacies 3 in Table 1; Figure 4C) has been observed, above which peloidal limestones (lithofacies 2 in Table 1; Figure 4B) are found, laterally changing to crinoidal limestones (lithofacies 1 in Table 1; Figure 4D). In the SE section, there are megaripples and herringbone cross-lamination within lithofacies 1. In both sections, SE and R (Figures 2 and 3), the top of lithofacies 1 is irregular. Furthermore, the R section shows that crinoidal limestones (lithofacies 1 in Table 1) are affected by normal paleofaults, as well as the presence of neptunian dykes filled

with pelagic lithologies (mudstone and wackestone of filaments, peloids, and radiolarians, which are always red in color, similar to those observed in the condensed levels above them; Figure 4E,F).

At the G, CM, and LP sections (Figures 2 and 3), the lower Pliensbachian (Ibex Zone) is recorded in peloidal limestones (lithofacies 2 in Table 1; Figure 4B,C). In the G section, this lithofacies shows an irregular morphology at its top, which is affected by a paleofault. At the CM and LP sections, peloidal limestones (lithofacies 2 in Table 1) are disposed on cherty limestones (lithofacies 4 in Table 1); at their top, a well-developed hardground is detected. In the LP section, lithofacies 2 (peloidal limestones) shows in its upper part some thin levels of nodular limestones less than 10 cm thick (lithofacies 5 in Table 1; Figure 4E). In the R and C sections, peloidal limestones (lithofacies 2 in Table 1; Figure 4B,C) are recorded in the Jamesoni Zone.

In the upper Pliensbachian, mainly in the Lavinianum Zone, nodular limestones (lithofacies 5 in Table 1; Figure 4E) (ILL and SE sections; Figures 2 and 3) and hardgrounds and condensed levels (lithofacies 6 in Table 1, Figure 4F) (SE, G, R, and C sections) are recorded. The nodular limestones show thickness that changes between 50 cm to 2 m from one section to the other. They are stratified with beds whose bottom and top are clearly delimited. The nodules, of cm size, were deposited with their major axis parallel to the bedding and locally embedded in a micrite red matrix. Lithofacies 6, in the R section, would be regarded as the whole Lavinianum Zone, while in the SE, G, and C sections, they would represent the lowest part of this zone (Figure 3). In the C section, above lithofacies 6 (hardgrounds and condensed levels) there is a decimetric level showing peloidal packstone/grainstone (lithofacies 2 in Table 1; Figure 4B). In the BA section, lithofacies 6 (hardgrounds and condensed levels) has been dated as the lower part of the Algovianum Zone. Finally, at the CM section, in the lower part of the Lavinianum Zone, a decimetric level of crinoidal grainstone (lithofacies 1 in Table 1) has been dated, on top of which a hardground appears.

Except for the LP and R sections, in the remaining sections (Figures 2 and 3) the rest of the upper Pliensbachian (Algovianum and Emaciatum zones) are represented by marls and marly limestone alternance (lithofacies 7 in Table 1; Figure 4G). At the LP section, crinoidal limestones (lithofacies 1 in Table 1) are attributed to the Algovianum Zone; at their top, there is a thin level of cherty limestones. Over this cherty limestone level, marls and marly limestone alternance is shown. In the R section, the Algovianum Zone is represented by peloidal limestone (lithofacies 2 in Table 1). Over these lithofacies, a marl and marly limestone alternance crops out (lithofacies 7 in Table 1). In the G section, at the top of nodular limestones (lithofacies 5 in Table 1) with several hardgrounds (Figure 2), dark marls (lithofacies 8 in Table 1) crop out (Figure 4H).

4.3. Stratigraphic Unconformities

The boundary between the algal laminites of the lower member of the Gavilán Fm and the limestones of the middle member were not studied in the stratigraphic sections considered in this paper. The data related to algal laminites and R1 unconformity used in the current paper were taken from [31].

The R2 unconformity is observed in the ILL, BA, G, CM, LP, R, and C sections as a sharp facies change. In the ILL section, such unconformity is represented by a change from crinoidal limestones with breccias to peloidal limestones. On the other hand, in the BA, G, CM, and LP sections, a facies change is well recognizable from cherty limestones to crinoidal limestones (BA section) or peloidal limestones (G, CM, and LM sections) (Figure 3). At the R and C sections, the boundary between peloidal limestones and crinoidal limestones (R section) and cherty limestones (C section) may represent this R2 discontinuity. It was not possible to detect if there is a gap associated with this discontinuity in any of these sections. In the M and PR sections, a marl and marly limestone alternance dated as upper Ibex and Davoei zones or upper Pliensbachian covers the cherty limestones (Figure 3). In

these last sections, the hiatus related to R2 would comprise most of the Ibex Zone up to the Lavinianum Zone.

The R3 unconformity in the ILL section shows a hardground (lithofacies 6 in Table 1) overlain by nodular limestones (lithofacies 5 in Table 1). The ammonite content enabled the detection of a hiatus spanning the complete Davoei Zone [37]. In the SE and R sections, the top of the crinoidal limestones (lithofacies 1 in Table 1) shows an irregular (erosional) geometry; moreover, in the R section, this unconformity surface is affected by paleofaults covered by a post-faulted condensed level and rocks attributed to the Zegrí Fm (Figure 3). In this section, on top of the irregular surface there is a condensed level, 5 to 10 cm thick, that has been dated as Lavinianum Zone [37]; in this condensed level, numerous belemnite fragmocones have been found with a dominant N20–30° E orientation (Figure 5A). At the G and CM sections, the top of the peloidal limestones also shows a hardground. In the G section, this surface is affected by paleofaults, and a typical ammonite association corresponding to the uppermost of the Ibex Zone is found. In addition, the condensed level above this hardground contains *Fuciniceras lavinianum* and *Protogrammoceras celebratum* of the Lavinianum Zone; hence, the hiatus associated with this discontinuity includes the Davoei Zone. The hardground observed on the top of the peloidal limestones in the CM section was dated as the upper part of the Ibex Zone, and the crinoidal limestones on that surface were attributed to the base of the Lavinianum Zone [37]; hence, the hiatus related to R3 unconformity in these sections comprises the Davoei Zone.

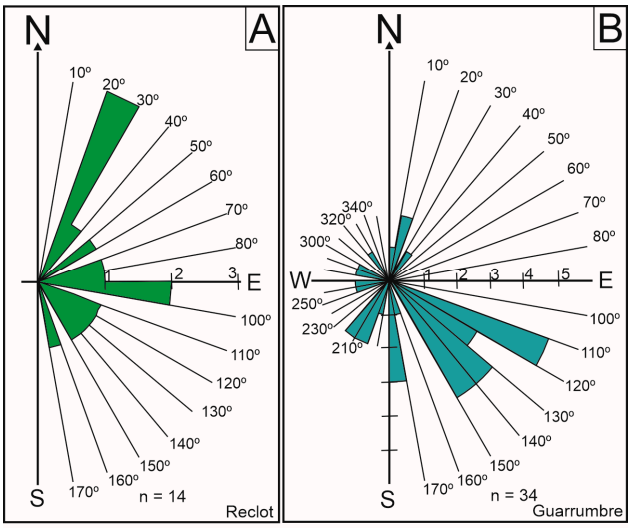

Figure 5. Paleocurrents deduced from the belemnites in (**A**) the Reclot (R) section and (**B**) the Guarrumbre (G) section. Both diagrams show results produced after the correction of the dip to the stratification.

The R4 unconformity was only recorded in the BA and LP sections (Figure 3). In both cases, it is a hardground with Fe-oxide thin crusts, bioturbation (e.g., Thalassinoides) and borings (Gastrochaenolites), and some ammonites (*Prodactylioceras davoei*) are also recorded. In the BA section, a condensed level with *Arieticeras algovianum* and *Arieticeras bertrandi* is found over this hardground. Therefore, the hiatus related to this discontinuity comprises the entire Lavinianum Zone.

The R5 unconformity is recorded in the SE, G, CM, and C sections (Figure 3). Excluding the CM section, the rest of the sections show a hardground developed over a condensed level that belongs to the lowermost Lavinianum Zone [37]. In the CM section, the hardground lies on top of a crinoidal grainstone level. In this hardground, ammonites from the lower part of the Lavinianum Zone have been found [37]. In addition, in the G section, numerous belemnite fragmocones have been observed associated with this hardground, showing a dominant orientation of N110–120° E and a second main direction between N130–150° E (Figure 5B). The materials overlying the hardground, characterizing

the R5 unconformity, consist of marls and marly limestone alternance belonging to the Algovianum Zone except in the SE section with nodular limestones corresponding to the Lavinianum Zone [37]. The hiatus related to this discontinuity comprises the middle and upper part of the Lavinianum Zone (Figure 3).

4.4. Isotope Geochemistry

4.4.1. Mingarrón (M) Section

A total of 66 samples were analyzed in this stratigraphic section (Table S1). Of these, 48 samples were taken from lithofacies 7, marls and marly limestone alternance (Table 1; Figure 4G), and the top 18 were taken from lithofacies 8 (dark marls; Table 1; Figure 4H). The $\delta^{13}C$ values in the bulk sample vary between 2.74‰ and −0.61‰ (Figure 6), with an average value of 1.08‰ and a standard deviation of 0.525. The variability of these data is much lower than that shown by Mercuzot et al. [10] for the Amellago–Ikis section, which shows a range of variation between 3.38‰ and −4.28‰ (Table 2). In the NJT5a Subzone of the M section (Figure 6), the values of this isotope ratio in the bulk sample range from −0.61 to 1.22‰, with an average value of 0.84‰; the standard deviation is 0.474. At the base of the NJT5a Subzone, there is a significant decrease in $\delta^{13}C$ values ranging from 1.22‰ to −0.61‰ (Figure 6). In the NJT5b Subzone, the minimum and maximum $\delta^{13}C$ values are −0.05‰ and 1.13‰ respectively; the average value is 0.74‰ and the standard deviation is 0.292. Finally, in the NJT6 Zone (Figure 6) the C isotope ratio values range from 0.11‰ to 2.74‰, with an average value of 1.37‰ and a standard deviation of 0.493. At the base of the NJT6 Zone, a change in the ratio values of the carbon isotopes is detected, from 1.07‰ (CO-45) to −0.05‰ (CO-47) (Table S1). In the rest of the zone, from this excursion onwards, a general increasing trend in $\delta^{13}C$ values is observed, reaching a plateau at the transit between the NJT6 and NJT7 zones (Figure 6).

The $\delta^{18}O$ values range from −1.44‰ to −3.58‰ (Figure 6), with an average value of −2.46‰ and a standard deviation of 0.398. This variability in isotope ratio values is unremarkable compared with that presented by Mercuzot et al. [10], −1.75 and −6.34‰ (Table 2). This isotope ratio in the NJT5a Subzone presents values between −2.10 and −3.20‰ (Figure 6), with an average value of −2.41‰ and a standard deviation of 0.309. As in the $\delta^{13}C$, at the base of the NJT5a Subzone, the $\delta^{18}O$ shows a punctual decrease in values, from −2.19‰ to −3.20‰ and back to −2.15‰. In the NJT5b Subzone (Figure 6), the $\delta^{18}O$ values range from −3.58‰ to −1.91‰, with an average value of −2.78‰; the standard deviation is 0.352. Finally, in the NJT6 Zone (Figure 6) the minimum and maximum values are −2.92‰ and −1.44‰, respectively; the average value is −2.30‰ and the standard deviation is 0.343. While in the $\delta^{13}C$ values a change is shown (Figure 6), for the $\delta^{18}O$ values there is no significant change; the values range from −3.58‰ to −3.01‰ and back to −2.95‰.

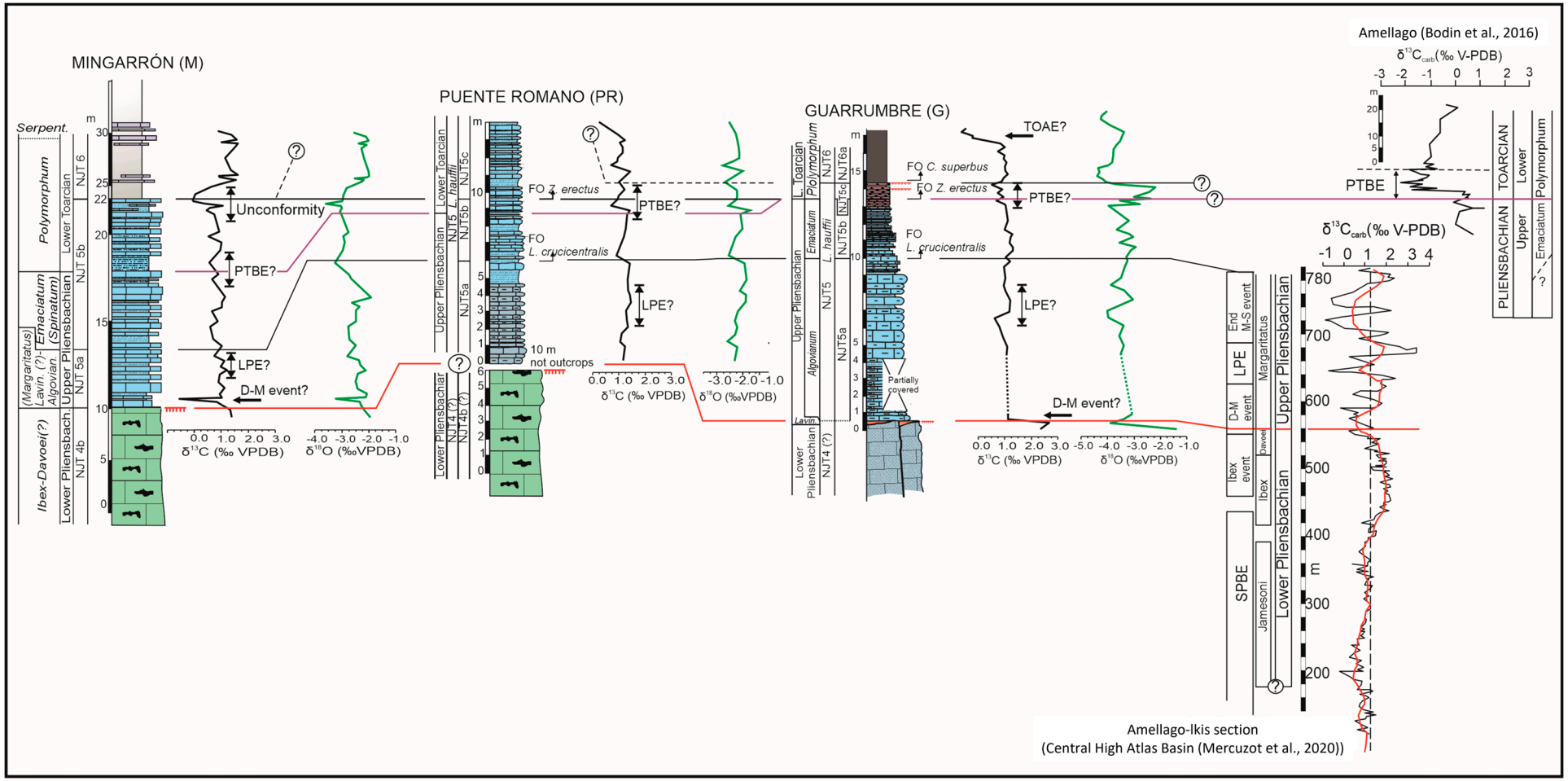

Figure 6. C and O isotope geochemistry for the Mingarrón (M), Puente Romano (PR), and Guarrumbre (G) sections and their correlation with the $\delta^{13}C$ curve for the Amellago–Ikis section [10] and the Amellago section [2]. The probable location of some Pliensbachian isotope events in the South Iberian Paleomargin is marked. For the three stratigraphic sections, see the lithofacies legend in Figure 2.

4.4.2. Puente Romano (PR) Section

In the PR section, 49 samples belonging to lithofacies 7 were analyzed (Table 1 and Table S1; Figure 4G). The $\delta^{13}C$ values in the bulk sample vary between 0.47‰ and 1.45‰ (Figure 6); the average value is 1.11‰ and the standard deviation is 0.168. In comparison with the variability of this isotope ratio shown by Mercuzot et al. [10] in the Amellago–Ikis section (Table 2), it is lower, with these values being within the range of variation shown by these authors. Coinciding with the FO of *L. crucicentralis* that marks the base of the NJT5b Subzone, a reduction in the value of this isotope ratio is detected, from 1.30‰ to 0.94‰, recovering the values until again reaching the value of 1.30‰ at the Pliensbachian–Toarcian boundary, around the FO of *Z. erectus* (NJT5c Subzone) where again there is a net change, decreasing to 0.80‰ (Figure 6). From here, the values of this isotope ratio increase once more to 1.31‰ at 11 m thickness. Then, again, a decrease in the $\delta^{13}C$ value is detected to 0.8‰ at 11.2 m thickness. The $\delta^{13}C$ value then increases to 1.17‰ at 13 m thickness and decreases to 0.47‰ at 14 m thickness. It increases one more time to 1.27‰ at 14.5 m thickness. From this level onwards, the $\delta^{13}C$ value remains at values close to the average (1.11‰ VPDB).

For the $\delta^{18}O$ value, the range of variation is between −2.76 and −0.67‰ (Figure 6), with an average value of −2.17 and a standard deviation of 0.331. As in the case of the $\delta^{13}C$, this variability in $\delta^{18}O$ values is lower than that obtained by Mercuzot et al. [10] (Table 2).

Table 2. Variability intervals of C and O isotope ratios obtained by different authors in Pliensbachian carbonates and comparison with the variability intervals in the Mingarrón (M), Puente Romano (PR), and Guarrumbre (G) sections studied in this paper.

	$\delta^{13}C$ (‰ V-PDB)	**$\delta^{18}O$ (‰ V-PDB)**
Basque–Cantabrian Basin, Reinosa Area [57]	−0.8 to 2.9	−3.2 to 0.7
Alpine–Mediterranean Domain [58]	−1.5 to 4.0	−3.7 to 0.5
Montcornet [9]	−4.5 to 2.5	−6.8 to −1.7
Amellago–Ikis (Central High Atlas, [10])	−4.28 to 3.38	−6.34 to −1.75
San Pedro de Moel, Lusitanian Basin [5]	−1.5 to 1.5	−5.61 to −1.39
Mingarrón (M)	−0.61 to 2.74	−3.58 to −1.44
Puente Romano (PR)	0.47 to 1.45	−2.76 to −0.67
Guarrumbre (G)	0.64 to 1.51	−4.39 to −2.24

4.4.3. Guarrumbre (G) Section

In section G, 38 samples were analyzed. Fourteen were taken in rocks with lithofacies 7; nine samples in the nodular limestones (lithofacies 5), and fifteen samples in the dark marls (lithofacies 8). The values of the $\delta^{13}C$ vary between 0.64 and 1.51‰, the average value is 1.12‰, and the standard deviation is 0.200. As in the two sections previously described, the range of variation in $\delta^{13}C$ is smaller than that detected by Mercuzot et al. [10], which is 7.58 ‰ (Table 2). The first detectable change in the $\delta^{13}C$ curve is observed between meters 6.5 and 7 (NJT5a Subzone), where the value of the isotope ratio increases from 0.64 to 1.21‰ (Figure 6). From this level onwards, the isotope ratio values remain around the average value, with a slight increase being detected coinciding with the nodular limestones (lithofacies 5 in Table 1). In these facies belonging to the NJT5c Subzone, the $\delta^{13}C$ reaches a value of 1.51‰, coinciding with the first of the hardgrounds detected (Figure 6). It drops to values of 0.88‰ coinciding with the second of the hardgrounds, which marks the boundary between the Pliensbachian and Toarcian, and the NJT5 and NJT6 zones, typically characterized by a negative carbon isotope excursion [2,10].

The $\delta^{18}O$ values vary between −4.39 and −2.24‰, with an average value of −3.49‰ and a standard deviation of 0.536. As in the previous cases, the range of variation in $\delta^{18}O$ is smaller than that shown by Mercuzot et al. [10] (Table 2). The variation curve of $\delta^{18}O$

shows that between meters 7 and 7.5, within the NJT5a Subzone, there is an increase in its value, from −4‰ to −3.14‰, to return to values of −3.84‰ at 8 m (Figure 6). From here, there is a progressive increase up to meter 11, belonging to the NJT5b Subzone, after which there is a reduction to a value of −3.90‰ in the bottom of the nodular limestones of the NJT5c Subzone (Figure 6). In these limestones, an average increase in the value of the $\delta^{18}O$ is detected until reaching values of −2.24‰ in the level whose top is the hardground 1 (Figure 6). From this point on, there is a decrease in the value of the $\delta^{18}O$ to −3.67, obtained in relation to the second of the hardgrounds detected in these facies, which marks the Pliensbachian–Toarcian and NJT5–NJT6 boundaries.

Table 2 shows the values of C and O isotope ratios obtained by several authors on Pliensbachian materials. The data of the same isotope ratios, shown above in each of the three sections considered in this paper, are within the ranges of variation obtained by these authors, and no isotope excursions were clearly detected.

5. Discussion

5.1. Sedimentary Environment

Several authors [31,36,37,39,41] have postulated that the algal laminite facies characterizing the lower member of the Gavilán Fm was deposited on a large, highly homogenous carbonate platform under very low-energy subtidal–intertidal conditions. The R1 unconformity records the first phase of disintegration of this large platform, which must have occurred at the Sinemurian–Pliensbachian transition (Figure 3). Because of this first extensional fracturing phase, the large carbonate platform was segmented, so that the ILL, R, and C sections developed in relatively more energetic shallow platform environments, where crinoidal limestones (ILL section) or peloidal limestones (R and C sections) were deposited in more and less energetic contexts, respectively. In the rest of the sections, cherty limestones rich in sponge spicules were deposited in open platform or hemipelagic contexts. In general, in relation to this R1 rupture, there was a deepening of the platform, although it was not of equal magnitude throughout the overall platform [59].

Due to the facies contrast detected in all the studied sections around the R2 unconformity, it can be established that it represents a new phase of disintegration of the carbonate platform, in the lower part of the Ibex Zone, coinciding with the FO of the *Biscutum grande* (NJT4b Subzone; Figure 3). In all the considered sections, the implantation of highly energetic shallow platform facies occurred, with a predominance of crinoidal limestones, which in the SE section even show herringbone-type structures. In the G, CM, and LP sections, there were less energetic environments, with the deposition of peloidal limestones. In the eastern sector, the C section, a deepening took place which favored the sedimentation of open platforms or hemipelagic facies (cherty limestones). In the M and PR sections, there is no sedimentary record on these cherty limestones (there are no facies attributable to the upper member of the Gavilán Fm), but on these lithofacies the Zegrí Fm (marls and marly limestone alternance) directly outcrops. Considering that shallow platform facies denoting high-energy conditions have been recorded in the rest of the sections, it is probable that both the M and PE sections were configured as somewhat higher areas in the context of the large and partitioned platform during the Ibex to the lower part of Algovianum zones; hence, the currents transported the sediment to relatively more sheltered areas. However, it cannot be discarded that sedimentation occurred in these two sections due to exposure to subaerial conditions, although, for the moment, there are no data to certainly support this hypothesis. With the exception of the C section, where deepening is recorded, and the M and PR sections, in the rest of the studied sections the extensional tectonic phase that gave rise to the R2 unconformity led to a shallowing of the platform and an increase in the energy of the environment interpreted as a Transgressive System Tract (TST) [31] and, therefore, a retrogradation of the platform.

The development of the R3 unconformity highlights a new stage of platform fracturing and increased compartmentalization, dated as the Ibex–Davoei zones boundary (Figure 3), which also coincides with the FO of *Lotharingius barozzi* (NJT4c Subzone). This led to the

development of different blocks, with disparate sedimentary evolutions between them [36]. Thus, in the ILL and CM sections, hardgrounds developed, indicating a stop in sedimentation spanning the Davoei Zone. In the SE, G, R, and C sections (Figure 3), we observe the development of an irregular morphology on top of crinoidal limestones, peloidal limestones, or cherty limestones, which has been interpreted as a paleokarst [31,34,36,60–62] and, therefore, the result of subaerial erosional processes. This paleokarst surface is affected by normal paleofaults, observable in the G and R sections. In the latter, it was described as an important network of neptunian dykes made up of peloidal red limestones (attributable to the Zegrí Fm) and even red limestones dated as Middle Jurassic [41]. Briefly, the fracturing phase associated with R3 entailed a generalized shallowing of the different developed blocks, which were subjected to subaerial conditions, with the occurrence of paleokarst or else with a standstill or extreme condensation of the sedimentation possibly associated with important currents flowing in several directions (Figure 5), perhaps conditioned by the distribution of the different blocks into which the primitive large carbonate platform was partitioned.

In the BA and LP sections, there is no record of the R3 unconformity. In the BA section, the crinoidal limestones were also deposited during the Davoei Zone (Figure 3). In the LP section, coinciding with the Ibex–Davoei zones boundary, a level with nodular limestones facies is recorded, which could be interpreted as an anomaly in the sedimentation of this part of the platform as a consequence of the extensive phase associated with the R3 unconformity, although no hiatus was detected. In both sections, a hardground is identified as coinciding with the boundary between the lower and upper Pliensbachian, which denotes the R4 unconformity. Associated with this hardground, a stratigraphic gap is recognized in these two sections, which spans the Lavinianum Zone (Figure 3). This R4 unconformity could be superimposed on the R3 unconformity in the rest of the studied sections, except for the BA and LP sections.

Over the R3 + R4 unconformities in the ILL, SE, G, CM, R, and C sections are nodular limestones (ILL section), condensed levels and nodular limestones (SE section), or condensed levels only (G, R, and C). These are facies that denote sedimentary condensation and characterize TST stages [31,37] normally related to energetic hemipelagic or pelagic marine contexts. The time interval represented by these materials is variable from one stratigraphic section to another, which corroborates that from the development of the R3 unconformity onwards, the disintegration of the platform was completed. Therefore, while in some sectors there were conditions of sedimentary condensation without interruption of sedimentation (ILL, SE, and R sections), leading to the development of the clearly pelagic facies typical of the Zegrí Fm (marls and marly limestone alternance), in others (G and C sections) a condensed level developed, representing the lower part of the Lavinianum Zone (Figure 3), at the top of which a new unconformity (R5) was recorded. This last unconformity (R5) is associated with a hiatus covering the middle and upper part of the Lavinianum Zone (practically the NJT4d and NJT4e subzones). In the CM section above R3 + R4, there are crinoidal limestones, which implies that this area was subjected to energetic platform conditions during the lower part of the Lavinianum Zone, i.e., while there was a shallowing trend in this section, in the rest of the sections a deepening is recorded.

The R5 unconformity, possibly also related to an extensional stage near the lower boundary of the NJT4d Subzone (Figure 3) led to a shutdown of sedimentation, which lasted until the middle and upper part of the Lavinianum Zone (NJT4d and NJT4e subzones). In general, coinciding with the base of the Algovianum Zone or the NJT5 Zone, the pelagic sedimentation typical of the Zegrí Fm became widespread (Figure 3), although with particularities in some sections such as BA, LP, R, or C. In the first of these sections, the implantation of the marls and marly limestone alternance facies occurred toward the middle part of the Algovianum Zone or toward the middle part of the NJT5a Subzone. These materials, with some ammonites and the absence of benthonic macroinvertebrates, are typical of pelagic or hemipelagic environments with different continental influences. In stages of greater continental influence, marly levels developed, while in periods of less

continental influence, calcareous marly levels were deposited [39,41]. In the LP section (Figure 3), in the early stages of the Algovianum Zone, crinoidal limestones in an energetic carbonate platform were deposited, which transitioned to cherty limestones at the end of this ammonite zone, i.e., a relative rise in sea level was recorded. The crinoidal platform becomes submerged, establishing a hemipelagic environment with abundant sponge spicules, which, due to the continued relative sea level rise, could eventually favor the development of a pelagic environment with deposits of the facies of marls and marly limestone alternance. At both R and C sections, the beginning of the Algovianum Zone corresponds to the deposition of peloidal limestones, with different development between the two sections (Figure 3). In both sections, a relatively low-energy shallow platform was implanted and drowned by the hemipelagic facies with alternating marls and marly limestones. This change in sedimentary environment occurred toward the end of the Algovianum Zone, coinciding with the FO of *Lotharingius crucicentralis* (Figure 3) in the R section, while in the C section, this process took place coinciding with the FO of *Lotharingius hauffii*, at the base of the Algovianum Zone.

5.2. Preservation of Primary C and O Isotope Signals

The correlation coefficient between the values of $\delta^{13}C$ and $\delta^{18}O$ from bulk samples has been considered an indicator of the intensity of diagenesis in carbonate rocks [10,63–65]. A low covariance between these values can be interpreted as a low level of diagenesis.

Thus, in the M and G sections (Figure 7A,C), the values of the correlation coefficient (R^2) are 0.359 and 0.334, respectively, indicating a low correlation between them and, therefore, a not very intense diagenetic alteration. On the other hand, in the PR section (Figure 7B) the value of this coefficient is 0.542, which is slightly higher than the previous ones. This could be interpreted as a sign that in the PR section, the diagenetic distortion of the initial isotopic values is slightly higher. In none of the three considered sections was the diagenetic alteration relatively high; therefore, the values of the isotope ratios can be equivalent to the original ones and reflect the isotopic composition of the original sediment.

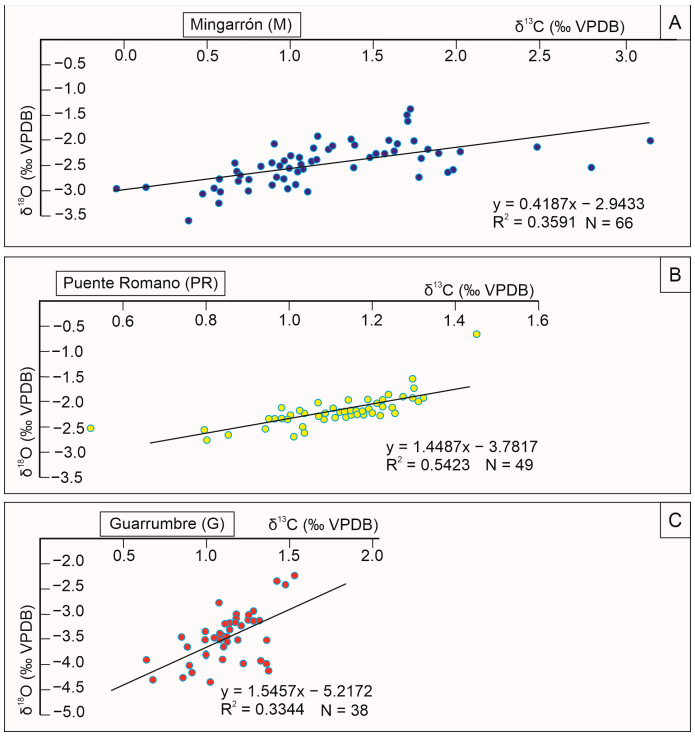

Figure 7. Correlation of the $\delta^{18}O$ (VPDB) vs. $\delta^{13}C$ (VPDB). (**A**) Mingarrón section; (**B**) Puente Romano section; and (**C**) Guarrumbre section. For each section, the correlation line and the correlation coefficient (R^2) were determined. N indicates the number of samples considered for each one.

5.3. Pliensbachian and C Isotope Events in the Subbetic and Correlation with the Tethyan Realm

The $\delta^{13}C$ data in the bulk sample from the M, PR, and G sections corresponding to the upper Pliensbachian (Figure 6) correlate with the curve of the Amellago–Ikis section (Central High Atlas Basin, [10]) and those of the Pliensbachian–Toarcian transition with the one proposed for the Amellago section [2], which is also located in the Central High Atlas Basin. Mercuzot et al. [10] identified the Davoei–Margaritatus Event (D-M Event) in the upper Pliensbachian, the late Pliensbachian Event (LPE), and the end Margaritatus–Spinatum Event (end M-S event) within the NJT5a Subzone. Also, in the Amellago section, the Pliensbachian–Toarcian Boundary Event (PTBE) was identified, coinciding with the uppermost NJT5b Subzone [2].

The $\delta^{13}C$ isotopic curve of the M, PR, and G sections (Figure 6) shows no clear excursions that can be accurately attributed to any of the above-mentioned events. In the M and G sections, a decrease in $\delta^{13}C$ isotope ratio values is observed at the base of the NJT5a Subzone, which could be cautiously correlated with the D-M Event (Figure 6). On the other hand, in the three sections considered in this chapter, a slight positive excursion in the $\delta^{13}C$ curve is detected toward the middle–upper part of the NJT5a Subzone, which, could be cautiously correlated with the LPE. Finally, the PTBE was identified in the G section by a weak negative excursion in the $\delta^{13}C$ isotope curve. This anomaly extends over the whole NJT5c Subzone. The values prior to this event coincide with the boundary between the NJT5c and NJT6a subzones in the G section (Figure 6). In the PR section, the PTBE could be reflected by a negative excursion located in the terminal part of the NJT5b Subzone, which would recover previous values of the isotope ratio at the base of the NJT5c Subzone. Finally, in the M section, this event could correspond to a weak decrease in the $\delta^{13}C$ isotope ratio values, coinciding with the boundary between the Spinatum and Polymorphum zones within the NJT5b Subzone.

5.4. The Demise of the Carbonate Platform: Tectonic versus Climate

The development of Lower Jurassic carbonate platforms in the western Tethys has been controlled by synsedimentary tectonic processes associated with the first stages of the breakup of Pangea [11,12,31,66–72]. These led to the development of blocks with differential subsidence where diverse types of carbonate sedimentation, shallow neritic in the higher areas of raised blocks, and sediments of hemipelagic nature in more subsiding parts were recorded. As a consequence of extensive synsedimentary tectonics, important paleogeographic and paleoceanographic changes developed, conditioning the marine circulation and water oxygenation levels [10–12,17,18,71]. From a paleoclimatic perspective, the Pliensbachian has been interpreted as a period of greenhouse climate, interrupted by short cold events [2,9,10,29]. These climatic changes have been recorded in O and C isotope curves obtained from sections of paleomargins of the Tethys and the Boreal domain ([10], and references therein).

In the SIP it has been clearly shown that the evolution of the Peritethys carbonate platform developed during the Lower Jurassic (Hettangian–Pliensbachian) was controlled by extensional tectonic events [31,35,36,70] reflected in the development of tilted blocks with different carbonate sediments (shallow and hemipelagic), among which there are lateral changes in facies, the presence of neptunian dykes of pelagic materials in shallow carbonates, synsedimentary normal faults affecting platform carbonates, and the development of paleokarst or stratigraphic units with variable thickness in the same tectonic unit.

The break-up process of this platform presented its first steps in the lower part of the Jamesoni Zone, near the Sinemurian–earliest Pliensbachian boundary [31]. These authors recorded an unconformity (named R1, Figure 3) at the top of the algal laminites in several units of the eastern Subbetic sector. This extensional phase can be correlated with the first stages of the opening of the Hispanic Corridor [12,13,17,18]. However, the peak stage of synsedimentary extensional tectonic activity that ended with the platform demise occurred between the lower part of the Ibex Zone (NJT4a–NJT4b subzones boundary; Figure 3) and

the Lavinianum–Algovianum zones boundary (NJT4–NJT5 zones boundary), from which a generalized homogenization of hemipelagic sedimentation occurred in the SIP. As shown in Figure 3, in this time interval, several unconformities (R2 to R5) have been detected in the different stratigraphic sections studied, as well as facies changes between them, paleokarst, hardgrounds and condensed sections, neptunian dykes, and synsedimentary extensional paleofaults. These data allow us to consider the presence of tilted blocks with simultaneous records of the relative sea level situation of opposite character. From the Algovianum Zone onwards, hemipelagic/pelagic sedimentation is established in the SIP, developing mainly an alternation of marl and marly limestones (lithofacies 7 in Table 1) during the rest of the late Pliensbachian.

In other areas on the margins of the Tethys, clear positive and negative trends in C and O isotope curves have been detected during the Pliensbachian and interpreted as a result of climatic changes [2,10–12,17,18,71]. In the M, PR, and G sections (Figure 6), the $\delta^{13}C$ and $\delta^{18}O$ curves do not clearly record the events detected in the upper Pliensbachian by those authors. As indicated in Section 5.3, the D-M Event, LPE, and PTBE (Figure 6) seem to be cautiously identified. During the studied time interval, the SIP was located close to the Hispanic Corridor (Figure 8). According to different authors [9,12,13,17,18,27], the breakup of Pangea, specifically the opening of the Hispanic Corridor, as well as the intense volcanic activity of the Central Atlantic Magmatic Province associated with this rifting process, were responsible for a sedimentary environment and a paleogeographic rearrangement that could have conditioned the marine circulation system. The SIP may have been an area where marine currents flowing from Panthalassa and others from the Tethys would have converged. These factors could have influenced the upper Pliensbachian isotope record since there would be a mixture of waters of different geochemical compositions, coming from both oceans, whose circulation would be controlled by the topography of the seafloor, articulated in incipient elevated zones (proto-seamounts) with shallow or condensed sedimentation and, even, emerged zones with paleokarst development and more subsident zones where hemipelagic/pelagic sedimentation would predominate.

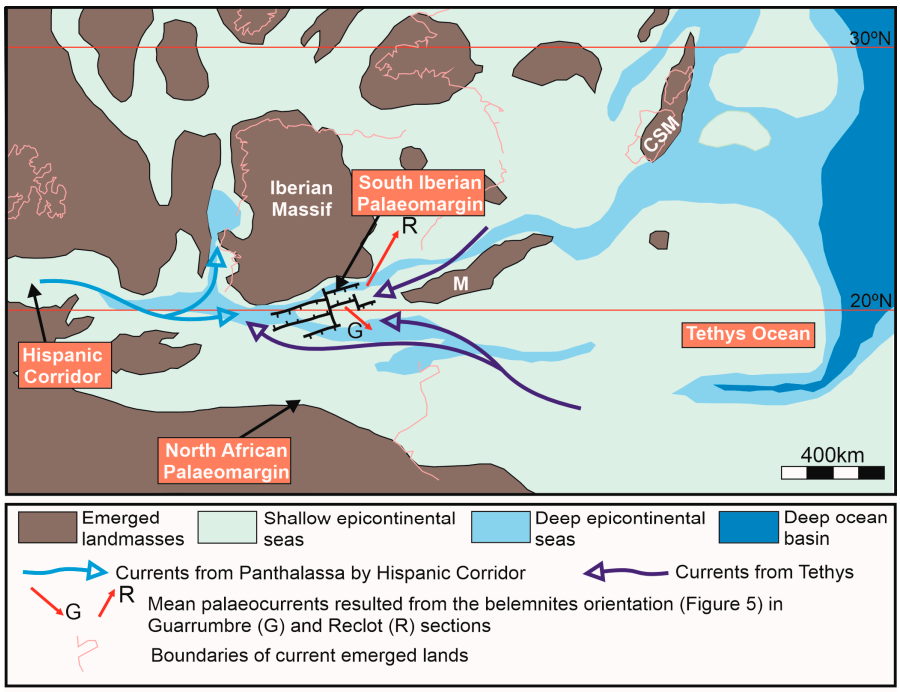

Figure 8. Paleogeographic map of the Pliensbachian with the location of the Hispanic Corridor and the South Iberian Paleomargin. The most probable marine currents are indicated. The figure is compiled from [13,17,27,35,36,73,74]. CSM: Corsica–Sardinia Massif; M: Mesomediterranean Microplate.

6. Conclusions

Ten stratigraphic sections of the Subbetic (Betic External Zones), whose sedimentary record is mainly Pliensbachian in age, although some of them also span the lower Toarcian, were studied. Eight different lithofacies were found: crinoidal limestones (grainstone), peloidal limestones (packstone/grainstone), breccias, cherty limestones (mudstone/wackestone), nodular limestones (wackestone/packstone), hardgrounds and condensed levels, marls and marly limestone alternance, and dark marls.

The demise of the Lower Jurassic shallow platform developed in the SIP was a complex process that was driven by extensional synsedimentary tectonics and led to the development of different tilted blocks. Several sedimentary environments developed, from the maintenance of shallow carbonate conditions in subtidal or intertidal environments to contexts without sedimentary record, with condensed sedimentation, with the development of hemipelagic environments, or even with the formation of paleokarst, which implies emersion and subaerial erosion. The following different tectonic phases occurred: (1) the Sinemurian–Pliensbachian transition (unconformity R1); (2) toward the lower part of the Ibex Zone, coinciding with the FO of the *Biscutum grande* (unconformity R2); (3) in the boundary between the Ibex and Davoei zones, coinciding with the FO of *Lotharingius barozii* (unconformity R3); (4) in the boundary between the lower and upper Pliensbachian (unconformity R4); and (5) near the lower boundary of the NJT4d Subzone (unconformity R5). After this last phase, hemipelagic sedimentation was generalized, with the development of a marl and marly limestone alternance facies.

In the M, PR, and G sections, the C and O isotope ratios in the bulk sample were studied, showing that in the three sections diagenesis scarcely modified the original isotopic signal, although in the PR section, the correlation coefficient between both isotope ratios is slightly higher than in the other two sections. The correlation of the $\delta^{13}C$ of these sections with that of Amellago–Ikis (Central High Atlas Basin, Morocco) highlights that in the Subbetic sections, there is no clear record of the different isotopic events analyzed by several authors. The Davoei–Margaritatus Event (D-M Event), the Late Pliensbachian Event (LPE), and the Pliensbachian–Toarcian Boundary Event (PTBE) could be cautiously identified.

The circumstance that C isotope events are not clearly recorded in these sections could be related to the fact that, during the studied time interval, the SIP was located close to the Hispanic Corridor, a strait associated with the beginning of the breakup of Pangea in the Early Jurassic. Therefore, there would be a convergence of marine waters with different chemistry, some coming from the Tethys and others from Panthalassa. In addition, the different stages of extension would facilitate the development of carbonate sedimentary environments, in which the relative changes in sea level would be frequent and would not favor their stability, to which important terrigenous influences could arrive (represented by the marl levels), modifying the isotope signal.

Supplementary Materials: The following supporting information can be downloaded at: https://www.mdpi.com/article/10.3390/min13111386/s1, Table S1: Geochemical data from $\delta^{13}C$ and $\delta^{18}O$ of the Mingarrón (M), Puente Romano (PR), and Guarrumbre (G) sections, Table S2: Distribution chart of the Guarrumbre section showing the results obtained from the semiquantitative analyses performed on 38 samples. Calcareous nannofossil zones and subzones identified in this work are indicated and calibrated to ammonite zones. Main events are written in bold. L. Pl. = Lower Pliensbachian, La = Lavianum. Assemblage abundance classes: A = abundant (10–15 specimens in each field of view), C = common (1–10 specimens in each field of view), F = few (1 specimen in 1–10 field/s of view), R = rare (1 specimen in 11–100 fields of view), and VR = very rare (1 specimen in more than 101 fields of view). Species abundance classes: A = abundant (1–5 specimens in each field of view), C = common (1 specimen in 2–10 fields of view), F = few (1 specimen in 10–30 fields of view), R = rare (1 specimen in 31–100 fields of view), and VR = very rare (1 specimen in more than 101 fields of view). Preservation classes: G = good (the majority of the specimens show their diagnostic characteristics and only some of them are slightly etched and/or overgrown), M = moderate (the majority of the specimens are recognizable, even if some of them are etched and/or overgrown and/or fragmented), B = poor (the majority of the specimens are

heavily etched or/and overgrown and/or fragmented and the identification of the species is sometimes difficult), and VB = very poor (only a few specimens are recognizable).

Author Contributions: Conceptualization, L.M.N., J.M.M., M.R. and P.A.R.-O.; methodology, L.M.N., J.M.M., M.R., P.A.R.-O. and Á.F.; writing—original draft preparation, L.M.N., J.M.M., M.R. and Á.F.; writing—review and editing, all the authors; project administration, L.M.N. and M.R. All authors have read and agreed to the published version of the manuscript.

Funding: This research was funded by the FEDER UJA 2020 PROJECT—1380715; Research Group RNM-200 (Junta de Andalucía): 1380715; and Research project PY20_00111 (Junta de Andalucía).

Data Availability Statement: The data used to make this contribution are set out therein as well as in the supplementary materials that accompany it.

Acknowledgments: The authors wish to acknowledge Antonio Piedra-Martínez and Mª José Campos, Technicians of the Laboratory of Geology (University of Jaén), and Samuel Almeida-Martín, from the Geology Area (University Rey Juan Carlos). We thank the reviewers of this manuscript for their comments, which have substantially improved it.

Conflicts of Interest: The authors declare no conflict of interest.

Appendix A

Alphabetical listing including all the calcareous nannofossil species cited in the text with full author citations.

Biscutum grande Bown 1987

Calcivascularis jansae Wiegand 1984 (=*Mitrolithus jansae* sensu Bown and Young in Young et al., 1986)

Carinolithus superbus (Deflandre, 1954) Prins in Grün et al., 1974

Lotharingius crucicentralis (Medd, 1971) Grün and Zweili, 1980

Lotharingius hauffii Grün and Zweili, 1974, emend. Goy, 1979

Schizosphaerella punctulata Deflandre and Dangeard, 1938

Zeugrhabdotus erectus (Deflandre, 1954) Reinhardt, 1965

References

1. Korte, C.; Hesselbo, S.P. Shallow marine carbon and oxygen isotope and elemental records indicate icehouse-greenhouse cycles during the Early Jurassic. *Paleoceanography* **2011**, *26*, PA4219. [CrossRef]
2. Bodin, S.; Krencker, F.-N.; Kothe, T.; Hoffmann, R.; Mattioli, E.; Heinhofer, U.; Kabiri, L. Perturbation of the carbon cycle during the late Pliensbachian—Early Toarcian: New insight from high-resolution carbon isotope records in Morocco. *J. Afr. Earth Sci.* **2016**, *116*, 89–104. [CrossRef]
3. van de Schootbrugge, B.; McArthur, J.M.; Baley, T.R.; Rosental, Y.; Wright, J.D.; Miller, K.G. Toarcian Anoxic Event: An assessment of global using belemnite C isotope records. *Paleoceanography* **2005**, *20*, 1–10. [CrossRef]
4. van de Schootbrugge, B.; Richoz, S.; Pross, J.; Luppold, F.W.; Hunze, S.; Wonik, T.; Blau, J.; Meister, C.; van der Weijst, C.M.H.; Suan, G.; et al. The Schandelah Scientific Drilling Project: A new reference core from northern Germany for understanding repeated Early Jurassic ocean anoxia. *Newsl. Stratigr.* **2019**, *52*, 249–296. [CrossRef]
5. Duarte, L.V.; Comas-Rengifo, M.J.; Silva, R.L.; Paredes, R.; Goy, A. Carbon isotope stratigraphy and ammonite biochronostratigraphy across the Sinemurian-Pliensbachian boundary in the western Iberian margin. *Bull. Geosci.* **2014**, *89*, 719–736. [CrossRef]
6. Franceschi, M.; Dal Corso, J.; Posenato, R.; Roghi, G.; Masetti, D.; Jenkyns, H.C. Early Pliensbachian (Early Jurassic) C-isotope perturbation and the diffusion of the *Lithiotis* Fauna: Insights from the western Tethys. *Palaeogeogr. Palaeoclimatol. Palaeoecol.* **2014**, *410*, 255–263. [CrossRef]
7. Gómez, J.J.; Goy, A.; Canales, M.L. Seawater temperature and carbon isotope variations in belemnites linked to mass extinction during the Toarcian (Early Jurassic) in Central and Northern Spain. Comparison with other European sections. *Palaeogeogr. Palaeoclimatol. Palaeoecol.* **2008**, *258*, 28–58. [CrossRef]
8. Gómez, J.J.; Comas-Rengifo, M.J.; Goy, A. Palaeoclimatic oscillations in the Pliensbachian (Early Jurassic) of the Asturian Basin (Northern Spain). *Clim. Past.* **2016**, *12*, 1199–1214. [CrossRef]
9. Bougeault, C.; Pellenard, P.; Deconink, J.-F.; Hesselbo, S.P.; Dommergues, J.-L.; Bruneau, L.; Cocquerez, T.; Laffont, R.; Huret, E.; Thibault, N. Climatic and palaeoceanographic changes during the Pliensbachian (Early Jurassic) inferred from clay mineralogy and stable isotope (C-O) geochemistry (NW Europe). *Glob. Planet. Chang.* **2017**, *149*, 139–152. [CrossRef]

10. Mercuzot, M.; Pellenard, P.; Durlet, C.; Bougeault, C.; Meister, C.; Dommergues, J.-L.; Thibault, N.; Baudin, F.; Mathieu, O.; Bruneau, L.; et al. Carbon-isotope events during the Pliensbachian (Lower Jurassic) on the African and European margins of the NW Tethyan Realm. *Newsl. Stratigr.* **2020**, *53*, 41–69. [CrossRef]
11. Léonide, P.; Floquet, M.; Durlet, C.; Baudin, F.; Pittet, B.; Lécuyer, C. Drowning of a carbonate platform as a precursor stage of the Early Toarcian global anoxic event (Southern Provence sub-Basin, South-east France). *Sedimentology* **2012**, *59*, 156–184. [CrossRef]
12. Schöllhorn, I.; Adatte, T.; Van de Schootbrugge, B.; Houben, A.; Charbonier, G.; Janssen, N.; Föllmi, K.B. Climate and environmental response to the break-up of Pangea during the Early Jurassic (Hettangian-Pliensbachian); the Dorset coast (UK) revisited. *Glob. Planet. Chang.* **2020**, *185*, 103096. [CrossRef]
13. Schöllhorn, I.; Adatte, T.; Charbonier, G.; Mattioli, E.; Spangenberg, J.E.; Föllmi, K.B. Pliensbachian environmental perturbations and their potential link with volcanic activity: Swiss and British geochemical records. *Sed. Geol.* **2020**, *406*, 105665. [CrossRef]
14. Ruebsam, W.; Reolid, M.; Mattioli, E.; Schwark, L. 2022 Organic carbon accumulation at the northern Gondwana paleomargin (Tunisia) during the Toarcian Oceanic Anoxic Event: Sedimentological and geochemical evidence. *Palaeogeogr. Palaeoclimatol. Plaeoecol.* **2022**, *586*, 110781. [CrossRef]
15. Wilmsen, M.; Neuweiler, F. Biosedimentology of the Early Jurassic post-extinction carbonate depositional system, central High Atlas rift basin, Morocco. *Sedimentology* **2008**, *55*, 773–807. [CrossRef]
16. Silva, R.L.; Duarte, L.V.; Wach, G.D.; Ruhl, M.; Sadki, D.; Gómez, J.J.; Hesselbo, S.P.; Xu, W.M.; O'Connor, D.; Rodrigues, B.; et al. An Early Jurassic (Sinemurian-Toarcian) stratigraphic framework for the occurrence of Organic matter Preservation Intervals (OMPIs). *Earth-Sci. Rev.* **2021**, *221*, 103780. [CrossRef]
17. Dera, G.; Pucéat, E.; Pellenard, P.; Neige, P.; Delsate, D.; Joachimski, M.M.; Reisberg, L.; Martinez, M. Water mass exchange and variations in seawater temperature in the NW Tethys during the Early Jurassic: Evidence from neodymium and oxygen isotopes of fish teeth and belemnites. *Earth Planet. Sci. Lett.* **2009**, *286*, 198–207. [CrossRef]
18. Dera, G.; Pellenard, P.; Neige, P.; Deconinck, J.-F.; Pucéat, E.; Dommergues, J.-L. Distribution of clay minerals in Early Jurassic Peritethyan seas: Palaleoclimatic significance inferred from multiproxy comparisons. *Palaeogeogr. Palaeoclimatol. Palaeoecol.* **2009**, *271*, 39–51. [CrossRef]
19. Price, G.P.; Baker, S.J.; VanDeVelde, J.; Clémence, M.-E. High resolution carbon cycle and seawater temperature evolution during the Early Jurassic (Sinemurian-Early Pliensbachian). *Geochem. Geophys. Geosyst.* **2016**, *17*, 3917–3928. [CrossRef]
20. Deconink, J.-F.; Hesselbo, S.P.; Pellenard, P. Climatic and sea-level control of Jurassic (Pliensbachian) clay mineral sedimentation in the Cardigan Bay Basin, Llanbedr (Mochras Farm) borehole, Wales. *Sedimentology* **2019**, *66*, 2769–2783. [CrossRef]
21. Mattioli, E.; Pittet, B. Spatial and temporal distribution of calcareous nannofossils along a proximal-distal transect in the Lower Jurassic of the Umbria-Marche Basin (central Italy). *Palaeogeogr. Palaeoclimatol. Palaeoecol.* **2004**, *205*, 295–316. [CrossRef]
22. Tremolada, F.; van de Schootbrugge, B.; Erba, E. Early Jurassic schizosphaerellid crisis in Cantabria, Spain: Implications for calcification rates and phytoplankton evolution across the Toarcian oceanic anoxic event. *Paleoceanography* **2005**, *20*, PA2011. [CrossRef]
23. Fraguas, Á.; Young, J.R. Evolution of the coccolith genus *Lotharingius* during the Late Pliensbachian-Early Toarcian interval in Asturias (N Spain). Consequences of the Early Toarcian environmental perturbations. *Geobios* **2011**, *44*, 361–375. [CrossRef]
24. Fraguas, Á.; Comas-Rengifo, M.J.; Gómez, J.J.; Goy, A. The calcareous nannofossil crisis in Northern Spain (Asturias province) linked to the Early Toarcian warming-driven mass extinction. *Mar. Micropaleontol.* **2012**, *94*, 58–71. [CrossRef]
25. Fraguas, Á.; Gomez, J.J.; Comas-Rengifo, M.J.; Goy, A. Pliensbachian calcareous nannofossil paleoecology in the E Rodiles section (Asturias, N Spain): A key location connecting the Boreal and Tethyan realms. *Mar. Micropaleontol.* **2021**, *163*, 101962. [CrossRef]
26. Fraguas, Á.; Gómez, J.J.; Goy, A.; Comas-Rengifo, M.J. The response of calcareous nannoplankton to the latest Pliensbachian–early Toarcian environmental changes in the Camino Section (Basque Cantabrian Basin, northern Spain). *Geol. Soc. Lond. Spec. Publ.* **2021**, *514*, 31–58. [CrossRef]
27. De Lena, L.F.; Taylor, D.; Guex, J.; Bartolini, A.; Adatte, T.; van Acken, D.; Spangenberg, J.E.; Samankassou, E.; Vennemann, T.; Schaltegger, U. The driving mechanism of the carbon cycle perturbations in the late Pliensbachian (Early Jurassic). *Sci. Rep.* **2019**, *9*, 18430. [CrossRef]
28. Krencker, F.-N.; Fantasia, A.; El Ouali, M.; Kabiri, L.; Bodin, S. The effects of strong sediment-supply variability on the sequence stratigraphic architecture: Insights from early Toarcian carbonate factory collapses. *Mar. Pet. Geol.* **2022**, *136*, 105469. [CrossRef]
29. Bodin, S.; Fantasia, A.; Krencker, F.-N.; Nebsjerg, B.; Christiansen, L.; Andrieu, S. More gaps than record! A new look at the Pliensbachian/Toarcian boundary event guided by coupled chemo-sequence stratigraphy. *Palaeogeogr. Palaeoclimatol. Palaeoecol.* **2023**, *610*, 111344. [CrossRef]
30. Nieto, L.M.; Ruiz-Ortiz, P.A.; Rey, J. La ruptura de la plataforma carbonatada liásica en la Unidad de Jabalcuz (dominio intermedio, prov. de Jaén). *Geogaceta* **2002**, *32*, 279–281.
31. Ruiz-Ortiz, P.A.; Bosence, D.W.J.; Rey, J.; Nieto, L.M.; Castro, J.M.; Molina, J.M. Tectonic control of facies architecture, sequence stratigraphy and drowning of a Liassic carbonate platform (Betic Cordillera, Southern Spain). *Basin Res.* **2004**, *16*, 235–257. [CrossRef]
32. Ruiz-Ortiz, P.A.; Castro, J.M.; Arias, C.; Vilas, L.; Martín-Chivelet, J.; de Gea, G.A.; Molina, J.M.; Nieto, L.M.; Reolid, M.; Aguado, R.; et al. *The South Iberian Continental Margin, In The Geology of Iberia: A Geodynamic Approach, Regional Geology Reviews*; C. Quesada, C., Oliveira, T., Eds.; Springer: Berlin, Germany, 2019; pp. 190–205.

33. Jenkyns, H.C. The demise and drowning of Early Jurassic (Sinemurian) carbonate platforms: Stratigraphic evidence from the Italian peninsula, Sicily and Spain. *Atti Dei Convegni Lincei* **2020**, *335*, 55–82.
34. García-Hernández, M.; López-Garrido, A.C.; Rivas, P.; Sanz de Galdeano, C.; Vera, J.A. Mesozoic palaeogeographic evolution of the External Zones of the Betic Cordillera. *Geol. En Mijnb.* **1980**, *52*, 155–168.
35. Vera, J.A. Evolution of the South Iberian Contimental Margin. In *Peri-Tethyan Rift/Wrench Basins and Passive Margins*; Ziegler, P.A., Cavazza, A., Robertson, A.H.F., Crasquin-Soleau, S., Eds.; Mémoires du Muséum National d'Histoire Naturelle: Paris, France, 2001; Volume 186, pp. 109–143.
36. Vera, J.A. (Ed.) *Geología de España*; SGE-IGME: Madrid, Spain, 2004; p. 890.
37. Nieto, L.M.; Ruiz-Ortiz, P.A.; Rey, J.; Benito, M.I. Strontium-isotope stratigraphy as a constraint on the age of condensed levels: Examples from the Jurassic of the Subbetic Zone (southern Spain). *Sedimentology* **2008**, *55*, 1–29. [CrossRef]
38. Reolid, M.; Molina, J.M.; Nieto, L.M.; Rodríguez-Tovar, F.J. *The Toarcian Oceanic Anoxic Event on the South Iberian Palaeomargin*; Springer Briefs in Earth Sciences; Springer: Cham, Switzerland, 2018; 122p.
39. Molina, J.M. Análisis de Facies del Mesozoico en el Subbético Externo (Provincia de Córdoba y Sur de Jaén). Ph.D. Thesis, University of Granada, Granada, Spain, 1987.
40. Rey, J. Análisis de la Cuenca Subbética Durante el Jurásico y Cretácico en la Transversal Caravaca de la Cruz—Vélez Rubio. Ph.D. Thesis, University of Granada, Granada, Spain, 1993.
41. Nieto, L.M. La Cuenca Subbética Mesozoica en el Sector Oriental de las Cordilleras Béticas. Ph.D. Thesis, University of Granada, Granada, Spain, 1997.
42. Molina, J.M.; Nieto, L.M. Facies análisis of the lower-middle Toarcian in the External Subbetic (provinces of Murcia and Granada, Southern Spain): Palaeoenvironmental conditions. In Proceedings of the 3rd Workshop and Fieldtrip of IGCP 655 Toarcian Oceanic Anoxic Event: Impact on Marine Carbon Cycle and Ecosystems, Erlagen, Germany, 2–5 September 2019.
43. Hesselbo, S.P.; Ogg, J.G.; Ruhl, M. Chapter 26. The Jurassic Period. In *Geologic Time Scale 2020*; Gradstein, F.M., Ogg, J.G., Schmitz, M.D., Ogg, G.M., Eds.; Elsevier: Amsterdam, The Netherlands, 2020; Volume 2, pp. 955–1021. [CrossRef]
44. Ferreira, J.; Mattioli, E.; Sucherás-Marx, B.; Giraud, F.; Duarte, L.V.; Pittet, B.; Suan, G.; Hassler, A.; Spangenberg, J.E. Western Tethys Early and Middle Jurassic calcareous nannofossil biostratigraphy. *Earth-Sci. Rev.* **2019**, *197*, 102908. [CrossRef]
45. McArthur, J.M.; Howarth, R.J.; Bailey, T.R. Strontium isotope stratigraphy: LOWESS Version 3: Best fit to the marine Sr-isotope curve for 0-509 Ma and accompanying look-up table for deriving numerical age. *J. Geol.* **2001**, *109*, 155–170. [CrossRef]
46. Reolid, M.; Nieto, L.M.; Rey, J. Taphonomy of cephalopod assemblages from Middle Jurassic hardgrounds of pelagic swells (South-Iberian Palaeomargin, Western Tethys). *Palaeogeogr. Palaeoclimatol. Palaeoecol.* **2010**, *292*, 257–271. [CrossRef]
47. Bown, P.R.; Young, J.R. Techniques. In *Calcareous Nannofossil Biostratigraphy*; Brown, P.R., Ed.; Kluwer Academic: London, UK, 1998; pp. 16–28.
48. Perilli, N.; Fraguas, A.; Comas-Rengifo, M.J. Reproducibility and reliability of the Pliensbachian calcareous nannofossil biohorizons from the Basque-Cantabrian Basin (N Spain). *Geobios* **2010**, *43*, 77–85. [CrossRef]
49. Braga, J.C. Ammonites del Domerense de la Zona Subbética (Cordilleras Béticas, S de España). Ph.D. Thesis, University of Granada, Granada, Spain, 1983.
50. Jiménez, A.P. Estudio Paleontológico de los Ammonites del Toarciense Inferior y Medio de las Cordilleras Béticas (Dactyliocerati-dae e Hildoceratidae). Ph.D. Thesis, University of Granada, Granada, Spain, 1986.
51. Sandoval, J.; Bill, M.; Aguado, R.; O'Dogherty, L.; Rivas, P.; Morard, A.; Guex, J. The Toarcian in the Subbetic basin (southern Spain): Bio-events (ammonite and calcareous nannofossils) and carbon-isotope stratigraphy. *Palaeogeogr. Palaeoclimatol. Palaeoecol.* **2012**, *342–343*, 40–63. [CrossRef]
52. Reolid, M.; Mattioli, E.; Nieto, L.M.; Rodríguez-Tovar, F.J. The Early Toarcian Oceanic Anoxic Event in the External Subbetic (Southiberian Palaeomargin, Westernmost Tethys): Geochemistry, nannofossils and ichnology. *Palaeogeogr. Palaeoclimatol. Palaeoecol.* **2014**, *411*, 79–94. [CrossRef]
53. Elmi, S.; Rulleau, L.; Gabilly, J.; Mouterde, R. Toarcien. In *Biostratigraphie du Jurassique Ouest-Européen et Méditerranéen*; Carieu, E., Hantzpergue, P., Coord, Eds.; Bulletin du Centre de la Recherche Elf Exploration Production: Pau, France, 1997; Mémoire, 17; pp. 25–36.
54. Page, K.N. The Lower Jurassic of Europe: Its subdivision and correlation. *Geol. Surv. Den. Greenl. Bull.* **2003**, *1*, 23–59. [CrossRef]
55. Reolid, M.; Iwanczuk, J.; Mattioli, E.; Abad, I. Integration of gamma ray spectrometry, magnetic susceptibility and calcareous nannofossils for interpreting environmental perturbations: An example from the Jenkyns Event (lower Toarcian) from South Iberian Palaeomargin (Median Subbetic, SE Spain). *Palaeogeogr. Palaeoclimatol. Palaeoecol.* **2021**, *560*, 110031. [CrossRef]
56. Fraguas, Á.; Molina, J.M.; Nieto, L.; Reolid, M. *Dating the Colomera Section (Median Subbetic, SE Spain) Using Calcareous Nannofossils*; Libro de resúmenes de las XXXVII Jornadas de las Sociedad Española de Paleontología: Cuenca, Spain, 2022.
57. Rosales, I.; Quesada, S.; Robles, S. Primary and diagenetic isotopic signal in fossils and hemipelagic carbonates: The Lower Jurassic of northern Spain. *Sedimentology* **2001**, *48*, 1149–1169. [CrossRef]
58. Jenkyns, H.C.; Jones, C.E.; Gröcke, D.R.; Hesselbo, S.P.; Parkinson, D.N. Chemostratigraphy of the Jurassic System: Applications, limitations and implications for palaeoceanography. *J. Geol. Soc. Lond.* **2002**, *159*, 351–378. [CrossRef]
59. Baeza-Carratalá, J.F.; Reolid, M.; Giannetti, A.; Benavente, D.; Cuevas-González, J. Coupling of trace elements in brachiopod shells and biotic signals from the Lower Jurassic South-Iberian Palaeomargin (SE Spain): Implications for the environmental perturbations around the early Toarcian Mass Extinction Event. *Estudios Geológicos* **2021**, *77*, e141. [CrossRef]

60. García-Hernández, M.; López-Garrido, A.C.; Martín-Algarra, A.; Molina, J.M.; Ruiz-Ortiz, P.A.; Vera, J.A. Las discontinuidades mayores del Jurásico de las Zonas Externas de las Cordilleras Béticas: Análisis e interpretación de los ciclos sedimentarios. *Cuad. Geol. Ibérica* **1989**, *13*, 35–52.
61. Vera, J.A.; Ruiz-Ortiz, P.A.; García-Hernández, M.; Molina, J.M. Paleokarst and related sediments in the Jurassic of the Subbetic Zone, Southern Spain. In *Paleokarst*; James, N.P., Choquette, P.W., Eds.; Springer: New York, NY, USA, 1988; pp. 364–384.
62. Molina, J.M.; Ruiz-Ortiz, P.A.; Vera, J.A. A review of polyphase karstification in extensional tectonic regimes: Jurassic and Cretaceous examples. Betic Cordillera, southern Span. *Sedim. Geol.* **1999**, *129*, 71–84. [CrossRef]
63. Jenkyns, H.C.; Clayton, C.J. Black shales and carbon isotopes in pelagic sediments from the Tethyan Lower Jurassic. *Sedimentology* **1986**, *33*, 87–106. [CrossRef]
64. Duchamp-Alphonse, S.; Gardin, S.; Fiet, N.; Bartolini, A.; Blamart, D.; Pagel, M. Fertilization of the northwestern Tethys (Vocontian basin, SE France) during Valanginian carbon isotope perturbation: Evidence from calcareous nannofossils and trace element data. *Palaeogeogr. Palaeoclimatol. Palaeoecol* **2007**, *243*, 132–151. [CrossRef]
65. Aguado, R.; Company, M.; Castro, J.M.; de Gea, G.A.; Molina, J.M.; Nieto, L.M.; Ruiz-Ortiz, P.A. A new record of the Weissert episode from the Valanginian succession of Cehegín (Subbetic, SE Spain): Bio- and carbon isotope stratigraphy. *Cretac. Res.* **2018**, *92*, 122–137. [CrossRef]
66. Bernoulli, D.; Jenkyns, H.C. Alpine Mediterranean and Central Atlantic Mesozoic facies in relation to the early evolution of the Tethys. In *Modern and Ancient Geosynclinal Sedimentation*; Dott, R.H., Shaver, R.W., Eds.; SEPM, Special Publication: Claremore, OK, USA, 1974; Volume 19, pp. 129–160.
67. Elmi, S. Stages in the evolution of lete Triassic and Jurassic carbonate platforms: The western margin of the Subalpine basin (Ardeche, France). In *Carbonate platforms: Facies, Sequences and Evolution*; Tucker, M.E., Wilson, J.L., Crevello, P.D., Sarg, J.R., Read, J.F., Eds.; Special Publication of International Association of Sedimentologist: Oxford, UK, 1990; Volume 9, pp. 9–144.
68. Winterer, E.L.; Bosellini, A. Subsidence and sedimentation on Jurassic passive continental margin, Southern Alps, Italy. *Am. Assoc. Petrol. Geol. Bull.* **1981**, *65*, 394–421.
69. Rey, J. A Liassic isolated platform controlled by tectonics: South Iberian Margin, southeast Spain. *Geol. Mag.* **1997**, *134*, 235–247. [CrossRef]
70. Nieto, L.M.; Ruiz-Ortiz, P.A.; Rey, J.; Benito, M.I. La ruptura de la plataforma carbonatada del Lías Inferior en el Subbético Oriental (provincias de Murcia y Alicante): Distribución de facies y valores isotópicos del $^{87}Sr/^{86}Sr$, C y O. *Geotemas* **2004**, *7*, 171–176.
71. Krencker, F.-N.; Lindström, S.; Bodin, S. A major sea-level drop briefly precedes the Toarcian oceanic anoxic event: Implication from Early Jurassic climate and carbon cycle. *Sci. Rep.* **2019**, *9*, 12518. [CrossRef]
72. Marok, A.; Reolid, M. Lower Jurassic sediments from the Rhar Roubane Mountains (Western Algeria): Stratigraphic precisions and synsedimentary block-faulting. *J. Afr. Earth Sci.* **2012**, *76*, 50–65. [CrossRef]
73. Thierry, J. Middle Toarcian. In *Atlas Peri-Tethys Paleogeographical Maps*; Dercourt, J., Gaetani, M., Vrielynck, B., Barrier, E., Biju-Duval, B., Brunet, M.-F., Cadet, J.P., Crasquin, S., Sandulescu, M., Eds.; CCGM/CGMW: Paris, France, 2000; Volume I-XX, map 8 (40 co-authors).
74. Guiraud, R.; Bosworth, W.; Thierry, J.; Delplanque, A. Phanerozoic geological evolution of Northern and Central Africa: An overview. *J. Afr. Earth Sci* **2005**, *43*, 83–143. [CrossRef]